# Crystal Structures of Soybean β-Amylase Reacted with β-Maltose and Maltal: Active Site Components and Their Apparent Roles in Catalysis[†,‡]

Bunzo Mikami,[§,∥] Massimo Degano,[∥,⊥] Edward J. Hehre,[#] and James C. Sacchettini[*]

*Departments of Biochemistry and of Microbiology and Immunology, Albert Einstein College of Medicine, 1300 Morris Park Avenue, Bronx, New York 10461, and Research Institute for Food Science, Kyoto University, Uji, Kyoto 611, Japan*

*Received January 19, 1994; Revised Manuscript Received April 1, 1994*[⊗]

ABSTRACT: The crystal structures of catalytically competent soybean β-amylase, unliganded and bathed with small substrates (β-maltose, maltal), were determined at 1.9–2.2-Å resolution. Two molecules of β-maltose substrate bind to the protein in tandem, with some maltotetraose enzymic condensation product sharing the same binding sites. The β-amylase soaked with maltal shows a similar arrangement of two bound molecules of 2-deoxymaltose, the enzymic hydration product. In each case the nonreducing ends of the saccharide ligands are oriented toward the base of the protein's active site pocket. The catalytic center, located between the bound disaccharides and found deeper in the pocket than where the inhibitor α-cyclodextrin binds, is characterized by the presence of oppositely disposed carboxyl groups of two conserved glutamic acid residues. The OE2 carboxyl of Glu 186 is below the plane of the penultimate glucose residue (Glc 2) of bound maltotetraose, 2.6 Å from the oxygen atom of that ligand's penultimate α-1,4-glucosidic linkage. The OE2 carboxyl of Glu 380 lies above the plane of Glc 2, 2.8 Å from the O-1 atom of the more deeply bound β-maltose. Saccharide binding does not alter the spatial coordinates of these two carboxyl groups or the overall conformation of the 57-kDa protein. However, the saccharide complexes of the active enzyme are associated with a significant (10 Å) local conformational change in a peptide segment of a loop (L3) that borders the active site pocket. This "hinged" loop is in an open position, extending into solvent in the unliganded protein (and the solvent channel in the crystal) and in a closed position, forming part of the active site (through interactions of Asp 101 with Glc 1 and of Val 99 with Glc 4) in the enzyme/saccharide complexes. With loop 3 closed, van der Waals interactions between the methyl groups of Val 99 and those of Leu 383 shield the catalytic groups and the reaction center from solvent, presumably allowing an ordered water molecule located near Glu 380 to provide topological control of the steric outcome of hydrolysis/hydration reactions. Loop 3 in the open position is essential for reaction product release and departure.

β-Amylase (EC 3.2.1.2) is distinguished from other starch-hydrolyzing enzymes by its unique pattern of catalyzing the successive liberation of β-maltose from the nonreducing ends of α-1,4-linked outer starch chains and maltooligosaccharides as small as maltotriose. β-Amylase also promotes several less well-known reactions which follow other stereochemical paths. Thus, though the enzyme does not hydrolyze maltose (Marshall & Whelan, 1973; Kato et al., 1974; Genghof et al., 1978), it does convert the β-anomer of maltose to maltotetraose to a small extent by a condensation reaction that is the reversal of maltotetraose hydrolysis (Hehre et al., 1969). β-Amylase further catalyzes the slow irreversible hydration of maltal, an enolic glycosyl donor lacking α- or β-anomeric configuration, to form β-2-deoxymaltose (Hehre et al., 1986; Kitahata et al., 1991).

The 2-Å-resolution structure of soybean β-amylase has recently been described (Mikami et al., 1993) for a catalytically inhibited (–SH alkylated) preparation of the enzyme complexed with the competitive inhibitor, α-cyclodextrin. The 57-kDa protein forms a single domain comprising a canonical $(\alpha/\beta)_8$ barrel core plus a region of loops on the C-terminal side of the β-barrel; each loop connects the C-terminus of a β-strand to the N-terminus of the succeeding α-helix. A cleft in the protein surface, involving residues of the loop region and core, leads to an approximately 18-Å-deep pocket reaching to the carboxyl end of the β-barrel and containing the presumed reaction center. One wall of the pocket is formed by a conserved and potentially flexible loop segment, comprising residues 96–102 of loop 3, that extends into solvent (Mikami et al., 1993). On the basis of these features, the structure of soybean β-amylase resembles that of triosephosphate isomerase (Alber et al., 1981) rather than the multidomain structures of α-amylases or glucoamylase. The α-amylases have an $(\alpha/\beta)_8$ barrel catalytic domain, but their reaction centers are located in clefts open at both ends (Matsuura et al., 1984; Buisson et al., 1987). The deep pocket conformation found in β-amylase is present in glucoamylase, but the latter's catalytic domain has a different $(\alpha/\alpha$-barrel) structure (Aleshin et al., 1992).

We now report high-resolution crystal structures for catalytically active soybean β-amylase (SBA)[1] and for SBA

[†] This study was supported, in part, by Research Grant GM-45859 from the National Institutes of Health (to J.C.S.) and Research Grant DMB 89-04332 from the National Science Foundation (to E.J.H.).

[‡] Coordinates have been deposited in the Brookhaven Protein Data Bank under the file names 1BYA (unliganded SBA), 1BYB (SBA/maltose-H), 1BYC (SBA/maltose-L), and 1BYD (SBA/maltal).

[*] Address correspondence to this author at the Department of Biochemistry, Albert Einstein College of Medicine.

[§] Research Associate in Biochemistry and in Microbiology and Immunology, Albert Einstein College of Medicine; on leave from the Research Institute for Food Science, Kyoto University.

[∥] The first two authors contributed equally to this work.

[⊥] Research Associate in Biochemistry, Albert Einstein College of Medicine.

[#] Department of Microbiology and Immunology, Albert Einstein College of Medicine.

[⊗] Abstract published in *Advance ACS Abstracts*, May 15, 1994.

[1] Abbreviations: SBA, catalytically active soybean β-amylase; SBA/maltose and SBA/maltal, SBA infused with β-maltose or maltal [α-D-glucopyranosyl-(1 → 4)-D-glucal], respectively.

0006-2960/94/0433-7779$04.50/0 

Table 1: Data Collection and Refinement Statistics and Crystals of Catalytically Competent SBA Alone or Infused with β-Maltose or Maltal

| designation | SBA | SBA/maltose-H | SBA/maltose-L | SBA/maltal |
|---|---|---|---|---|
| crystal | 1 | 1 | 1 | 1 |
| applied substrate | none | β-maltose | β-maltose | maltal |
| soaking concn (mM) | | 200 | 8 | 100 |
| soaking conditions | | 1 h, 20 °C | 1 h, 20 °C | 40 min, 4 °C |
| cell dimensions | | | | |
| *a*, *b* (Å) | 86.2 | 86.2 | 86.2 | 86.4 |
| *c* (Å) | 144.5 | 144.4 | 144.5 | 145.3 |
| measured reflections | 219183 | 196202 | 180801 | 176655 |
| unique reflections | 45035 | 50275 | 42972 | 46480 |
| completeness for resolution range (%)[a] | 72 | 73 | 79 | 80 |
| residues/waters | 491/321 | 491/317[b] | 491/317[b] | 491/317 |
| sulfate ion | 1 | 1 | 1 | 1 |
| rms deviation from canonical stereochemistry | | | | |
| bond length (Å) | 0.020 | 0.017 | 0.017 | 0.018 |
| bond angle (deg) | 2.40 | 2.11 | 2.27 | 2.30 |
| *R*-factor (%) | 16.9 | 14.9 | 14.9 | 14.5 |
| resolution range in refinement (Å) | 9.0–2.2 | 9.0–1.9 | 9.0–2.2 | 9.0–2.2 |

[a] Completeness for data used in refinement. [b] One additional ordered water molecule is present when the electron density is fitted with the enzymic condensation product, maltotetraose.

complexes in crystals reacted with either β-maltose or maltal. Structural models of native soybean β-amylase and its complex with anomerized maltose at low (6 Å) resolution were previously described by Mikami et al. (1992). A difference Fourier map revealed the presence of two adjoining positive areas of electron density, each about the size of a maltose residue, located deep in the assumed active cleft. In addition, a negative density was evident "around loop 3" in the unliganded enzyme, together with a comparably sized positive peak about 8 Å away and close to the densities represented as bound maltose. The latter observations suggested possible movement of a polypeptide chain in the loop 3 region when maltose is bound; however, firm structural assignments based on fitting residues to the density peaks were not feasible. It seemed possible that clarification of these preliminary findings through analysis of crystal structures refined at high resolution might provide data of significance with respect to the enzyme's catalytic functioning.

The present structures of SBA complexes prepared with β-maltose and maltal allow the first detailed description of the composition and geometry of the active site of β-amylase. Aspects of the latter include the identity and disposition of the catalytic groups and saccharide ligands, the binding interactions of the ligands with protein residues, and the nature of the local conformational change in a segment of loop L3 in relation to substrate binding. The structural findings are discussed with respect to the ability of β-amylase to yield hydrolytic products of conserved (β) configuration from substrates differing in configuration at C-1 (Hehre et al., 1969, 1979, 1986; Kitahata et al., 1991) and also with regard to the action pattern of β-amylase on starch, including the inability to bypass α-1,6-linked branch points (Meyer et al., 1941; Sumner & French, 1956), and the potential to repeatedly cleave the same substrate chain (Bailey & French, 1957; Greenwood & Milne, 1968; Suganuma et al., 1980). New findings indicating that modification of the thiol groups of β-amylase, long known to inhibit catalysis, may do so by interfering with the movement of loop 3 are also discussed.

## EXPERIMENTAL PROCEDURES

*Crystals and Data Collection.* The trigonal crystals of SH-derivatized (nearly inactivated) β-amylase used in the previous study of the α-cyclodextrin complex (Mikami et al., 1993) were treated with dithiothreitol to remove the 2-mercaptoethanol ($-SCH_2CH_2OH$) adduct present on four of the protein's six cysteine thiol groups. The crystals, stored in 50% saturated ammonium sulfate, 0.1 M sodium acetate buffer (pH 5.4), 18 mM 2-mercaptoethanol, and 1 mM EDTA, were transferred to a solution of 50% ammonium sulfate, 0.1 M sodium acetate, and 1 mM EDTA, adjusted to pH 7.0, and then transferred to the same pH 7.0 solution containing 50 mM dithiothreitol and kept at 20 °C for 1 day. Preparatory to diffraction, the crystals were transferred to 50% saturated ammonium sulfate, 50 mM dithiothreitol, 1 mM EDTA, and 0.1 M sodium acetate solution at pH 5.4—either without ligand or containing 8 or 200 mM β-maltose or 100 mM maltal. The maltose, a highly purified, crystalline sample of the β-anomer, supplied by Dr. I. Wolff of the U.S. Department of Agriculture, was free of chromatographically detectable glucose or higher maltosaccharides; maltal, freshly prepared by catalytic deacetylation of the pure tetra-*O*-acetate and separated on a column of silica gel (Hehre et al., 1986), likewise was chromatographically pure. Each carbohydrate-containing soaking solution was prepared with 1 min of crystal addition. Data collection (at 20 °C) was begun after the crystal was soaked for 1 h at 20 °C (maltose) or 40 min at 4 °C (maltal). These treatments did not cause a significant change in cell dimension. Reduction with dithiothreitol did restore considerable catalytic activity; one crystal, assayed after diffraction data collection (35 h of X-ray irradiation), hydrolyzed amylopectin to form 83 μmol of maltose·$min^{-1}$·$mg^{-1}$ at pH 5.4 and 37 °C.

Diffraction intensity data were collected using a Siemens X-1000A multiwire area detector coupled with a Rigaku RU-200 rotating anode generator equipped with a graphite monochromator, operating at 40 kV and 150 mA. The crystal to detector distance was 18.5 cm in all cases. The detector 2θ angle was either 9° or 32°; the scan range was 0.25° per frame, and each frame was collected for 45 or 60 s. The collected data was processed by the XENGEN program (Siemens Inc., Madison, WI) to integrated intensities. Table 1 summarizes the cell parameters and data collection statistics for both the unliganded and complexed crystals of the active soybean β-amylase.

*General Refinement Method.* The structures in all instances were refined using molecular dynamics, energy minimization, and restrained least squares. The initial models used in the refinement contained only atoms of the protein component of our previously reported SBA/α-cyclodextrin complex (Mikami et al., 1993). The first macrocycle of refinement consisted of a simulated annealing procedure, using the SLOWCOOL

procedure as implemented in X-PLOR (Brünger, 1987, 1992), without modification; this was followed by five cycles of temperature factor refinement and manual model building using the program TOM, a derivative of FRODO (Jones, 1985). The second and subsequent macrocycles consisted of about 100 cycles of positional refinement, followed by 5–10 cycles of individual *B*-factor refinement, and manual model building. $[F_o] - [F_c]$ and $2[F_o] - [F_c]$ and simulated annealing omit electron density maps were used in the manual model building. To inspect the active site region, simulated omit maps were calculated—excluding from the calculation all atoms within a sphere large enough to encompass the entire active site. Water molecules were added when they appeared as a peak greater than at least three times the standard deviation of the map ($3\sigma$) in the $[F_o] - [F_c]$ electron density map and were less than 3.2 Å away from a hydrogen bond acceptor or donor (Smith et al., 1988). When the value of the conventional crystallographic *R*-factor had decreased to approximately 0.18, the energy minimization was substituted by a restrained least squares minimization, as implemented in the program TNT (Tronrud et al., 1988). From this point the positional parameters and temperature factors of the model atoms were refined simultaneously.

*Refinement of Unliganded SBA.* Although data were collected from a single crystal to a maximal resolution of 1.9 Å, the high *R*-merge values and a low percentage of completeness (68% to 1.9 Å) suggested the use in the refinement of the data only to 2.2 Å. After the first cycle, the *R*-factor decreased to 0.223 using the data between 9 and 2.2 Å. The four modified cysteine residues were changed to their actual free –SH form, and 318 water molecules and 1 sulfate ion were incorporated in the model during the following three refinement macrocycles. This resulted in the decrease of the *R*-factor to 0.202, using data in the same resolution range. Ordered solvent was then fitted inside the active site pocket, 16 water molecules in all. After two rounds of refinement, 10 cycles of *B*-factor refinement were carried out. This reduced the *R*-factor value to 0.180. Five more cycles, in turn releasing and restraining the protein geometry, reduced the *R*-factor to the final value of 0.169 for the data between 9.0 and 2.2 Å. The model, after seven refinement macrocycles, contains 491 amino acid residues (Ser 5 to C-terminal Gly 495), 321 water molecules, and 1 sulfate ion; it presents a deviation from the canonical bond lengths of 0.020 Å and a 2.403° rms deviation for the bond angles.

*Refinement of SBA/Maltose Complexes.* The crystal structures of the complexes, prepared by soaking two single crystals in β-maltose (nearly anomerically equilibrated by the end of the soak) at 8 mM (SBA/maltose-L) or 200 mM (SBA/maltose-H) concentration, were refined. After the first refinement macrocycle of SBA/maltose-H ($R = 0.233$, 9.0–2.5 Å), the $[F_o] - [F_c]$ map showed residues 96–103 of loop 3 to be in a conformation different from that found in the previously reported structure of the SBA/α-cyclodextrin complex (Mikami et al., 1993). The atoms of these residues were fit to the electron density, and water molecules were incorporated during several refinement macrocycles. The $[F_o] - [F_c]$ map at this stage suggested the presence of two β-maltose molecules in tandem. These two molecules were fitted and used in the subsequent refinement. However, in all following stages a positive peak in the $[F_o] - [F_c]$ map was observed in close proximity to C-1 (on the *si* side) of the second glucose unit and extending to the third glucose residue. This suggested the additional presence of the condensation product, maltotetraose, in the active site. We fitted the density with a maltotetraose molecule, and the electron density maps calculated after subsequent refinement showed a broad peak in the region previously fitted with the second glucose unit. This implied that both forms are present in the crystal used for the X-ray diffraction. The final model contains two β-maltose units and also a maltotetraose molecule plus one water with the latter molecule occupying approximately the position of the equatorial O-1 oxygen of the second glucose residue. The crystallographic *R*-factor for the model is 0.149 for the data between 9.0 and 1.9 Å (73% complete); rms bonds = 0.017 Å; rms angles = 2.110°.

SBA/maltose-L was refined by using the SBA/maltose-H model after the substrate and the water molecules in the active site were removed. $[F_o] - [F_c]$ and $2[F_o] - [F_c]$ maps calculated after the first refinement macrocycle ($R = 0.198$) clearly showed one β-maltose molecule at subsites 1 and 2 and the displaced loop 3 segment. After a further macrocycle of refinement, the electron density from an $[F_o] - [F_c]$ map showed unambiguously the location of the ligand, and it was fitted with four separate glucose units. Missing water molecules were also added. Inspection of the $2[F_o] - [F_c]$ electron density map calculated after the next macrocycle confirmed the correct positioning of three out of four glucose residues and the higher degree of disorder associated with the residue at position 3. From a positive peak of an $[F_o] - [F_c]$ electron density map it was possible to assess the α-1,4-glucosidic linkages between glucose residues 1 and 2 and between glucose residues 3 and 4. The maps calculated after the following refinement step showed a perfect analogy with the case of SBA/maltose-H regarding the presence of two β-maltose molecules and also maltotetraose plus a water molecule. The final model, containing 491 amino acids and either 2 β-maltose molecules and 317 water molecules or 1 maltotetraose and 318 waters, has an *R*-factor of 0.149 using data between 9.0 and 2.2 Å. The standard deviations for bond lengths and bond angles are 0.017 Å and 2.270°, respectively.

*Refinement of the SBA/Maltal Complex.* In the initial step the same procedure as in the case of SBA/maltose-L was followed. The *R*-factor was 0.175. Then the electron density inside the active site was fitted with four glucose units but lacking all the exocyclic oxygens. After restrained least squares refinement, the $[F_o] - [F_c]$ electron density map showed unambiguously the position of all the missing oxygens. No positive electron density peaks were detected near carbon atom 2 of the second and fourth glucose moieties. Only one positive peak of electron density, three times the standard deviation, was present between C-1 of glucose 1 and C-4 of glucose 2; and identical situation was present for glucose 3 and 4, indicating an α-1,4-glucosidic linkage between the units in each case. The model, containing two disaccharide ligands, was subjected to two macrocycles of refinement. No other significant electron density peaks were detected in the $2[F_o] - [F_c]$ and $[F_o] - [F_c]$ maps. The final model contains 491 amino acids, 2 2-deoxymaltose molecules, and 317 water molecules; it has an *R*-factor of 0.145 for data between 9.0 and 2.2 Å. The root mean square (rms) deviations on the bond lengths and bond angles are 0.018 Å and 2.298°, respectively.

## RESULTS

*Overall Structure of Active Soybean β-Amylase.* The crystal structures of SBA unliganded, complexed with maltose, and complexed with maltal have been refined to high resolution with acceptable *R*-factors and stereochemistry. Table 1 provides a summary of the data collection and refinement parameters for SBA, SBA/maltose-H, SBA/maltose-L, and

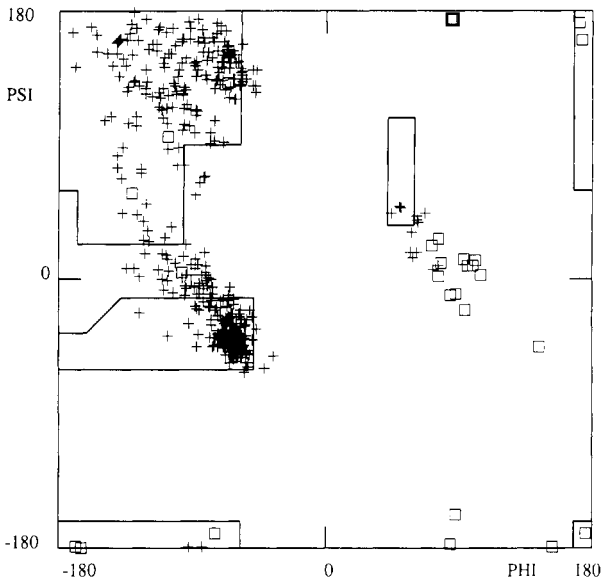


FIGURE 1: Ramachandran plot for the refined SBA/maltose-H structure. Glycines are plotted as squares; all other residues, as crosses. The $\phi$ and $\psi$ angles of all residues are in the allowable regions of low energy.

SBA/maltal. Figure 1 is a Ramachandran plot of the data for SBA/maltose-H which is representative of all four structures. The protein folds as a single domain consisting of an $(\alpha/\beta)_8$ barrel core plus a smaller loop region that covers the C-terminal end of the $\beta$-barrel. Each of this region's loops (several of considerable length) links the C-terminal residue of a $\beta$-strand to the N-terminus of the succeeding $\alpha$-helix. The surface of the region shows a cleft, bounded by loops L3 to L7, leading into a deep pocket whose base contains the C-termini of several $\beta$-strands, especially $\beta$-2, -5, -6, and -7. The overall structure of the unliganded, active SBA with free cysteine thiol groups is remarkably similar to that previously reported (Mikami et al., 1993) for the $\alpha$-cyclodextrin complex of a preparation of the SBA which had been modified by alkylation of four of its six –SH groups. There is likewise conservation of the overall structure among SBA, SBA/maltose-H, SBA/maltose-L, and SBA/maltal. The rms deviation among the three liganded complexes is 0.015 Å; that between unliganded SBA and the complexes is 0.081 Å. This heightened value is due to a notable local conformational change associated with substrate binding, involving a segment of peptide loop 3 that borders the active site; this change will be described in detail below.

*Identity and Disposition of Ligands in SBA Soaked with $\beta$-Maltose or with Maltal.* Electron density maps of the SBA complexes prepared with 8 or 200 mM $\beta$-maltose (SBA/maltose-L and SBA/maltose-H) show similar ligand density patterns, consistent with the shared occupancy of four "glucose subsites" between (a) two molecules of $\beta$-substrate bound in tandem with their nonreducing ends directed toward the base of the active site pocket and (b) one molecule of similarly oriented maltotetraose plus one molecule of water (enzymic condensation products).[2] In both situations, all D-glucopyranosyl units appear to be of $^4C_1$ conformation (Figure 2). Further, in the SBA/maltose-H complex (maltotetraose form) the torsional angles between Glc 1 and Glc 2 are $\phi = 67°$, $\psi = -151°$; between Glc 2 and Glc 3 are $\phi = 153°$, $\psi = 100°$; and between Glc 3 and Glc 4 are $\phi = 112°$, $\psi = -113°$. A nearly identical set of torsional angles is found in the SBA/maltose-L complex.

[2] Some occupancy of subsites Glc 1 and Glc 2 by a molecule of $\alpha$-maltose (formed by anomerization of the infused substrate) cannot be excluded at this level of resolution.

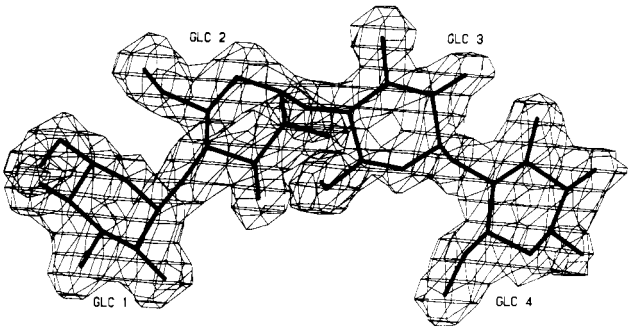


FIGURE 2: Stick model of maltotetraose fitted to the electron density of the $[F_o] - [F_c]$ omit map of the SBA/maltose-H complex.

A ribbon diagram of the structure of the SBA/maltose-H complex (Figure 3A) shows the four bound D-glucose units partly hidden behind a loop 3 segment that is closed on them. Figure 3B illustrates, by means of a section of the van der Waals surface of the SBA/maltose-H complex, that the four bound D-glucosyl units of the complex extend from the deepest part of the active site pocket, at the left (Glc 1), to the protein surface (Glc 4). The nonreducing end of Glc 1 binds under a ledge partly formed by protein residue Arg 420. Both Glc 1 and Glc 2 of the more deeply seated $\beta$-maltose molecule are located well below and behind the binding position of $\alpha$-cyclodextrin. Glc 3, the nonreducing moiety of the second bound $\beta$-maltose molecule, also is found below the deepest residue of bound $\alpha$-cyclodextrin; while Glc 4, the reducing moiety of the second $\beta$-maltose, binds between the locations of Glc 3 and 4 of the $\alpha$-cyclodextrin—not coincident with either. On the other hand, the $\alpha$-1,4-linkages of the $\beta$-maltose molecules run in the same interior-to-surface direction as those joining the three most deeply seated glucose units of bound $\alpha$-cyclodextrin. The methyl groups of Leu 383 which extend into the $\alpha$-cyclodextrin cavity at its O-2/O-3 end are evident.

The bound sugars Glc 1 and 4 are well ordered in both SBA/$\beta$-maltose complexes as judged from electron density maps; Glc 2 and Glc 3 are somewhat less well ordered. The omit maps show a peak of strong electron density at the axial O-1 position of Glc 2, suggesting the presence of maltotetraose (the enzymic condensation product) as a bound ligand[2] and also the possibility of slight movement in the O-1 region of Glc 2 and the O-4 region of Glc 3 whose C-1 atom is stabilized by glycosidic linkage to Glc 4. Mean *B*-factors for residues Glc 1 to Glc 4 were 14, 19, 27, and 27 Å$^2$, respectively.

The electron density map of SBA bathed with 100 mM maltal shows two molecules of 2-deoxymaltose (the enzymic hydration product) occupying the same four sites with their nonreducing ends directed toward the base of the active site. Only a small difference is found between all equivalent ring atoms of the bound saccharides of SBA/maltose-H and SBA/maltal (mean rms deviation 0.31 Å). The more deeply bound deoxymaltose molecule is of $\beta$-anomeric configuration; the more superficially bound one is the $\alpha$-anomer. No unreacted maltal substrate is detected; its hydration in the infused crystal would be expected to approach completion by the end of the soak period and the first few minutes of diffraction data collection, based on estimates using solution rate constants (Kitahata et al., 1991).

*Nature and Disposition of the Catalytically Active Residues.* Two oppositely disposed carboxyl groups, from Glu 186 and Glu 380, are identified as most likely responsible for the chemistry of catalysis by $\beta$-amylase. As illustrated in

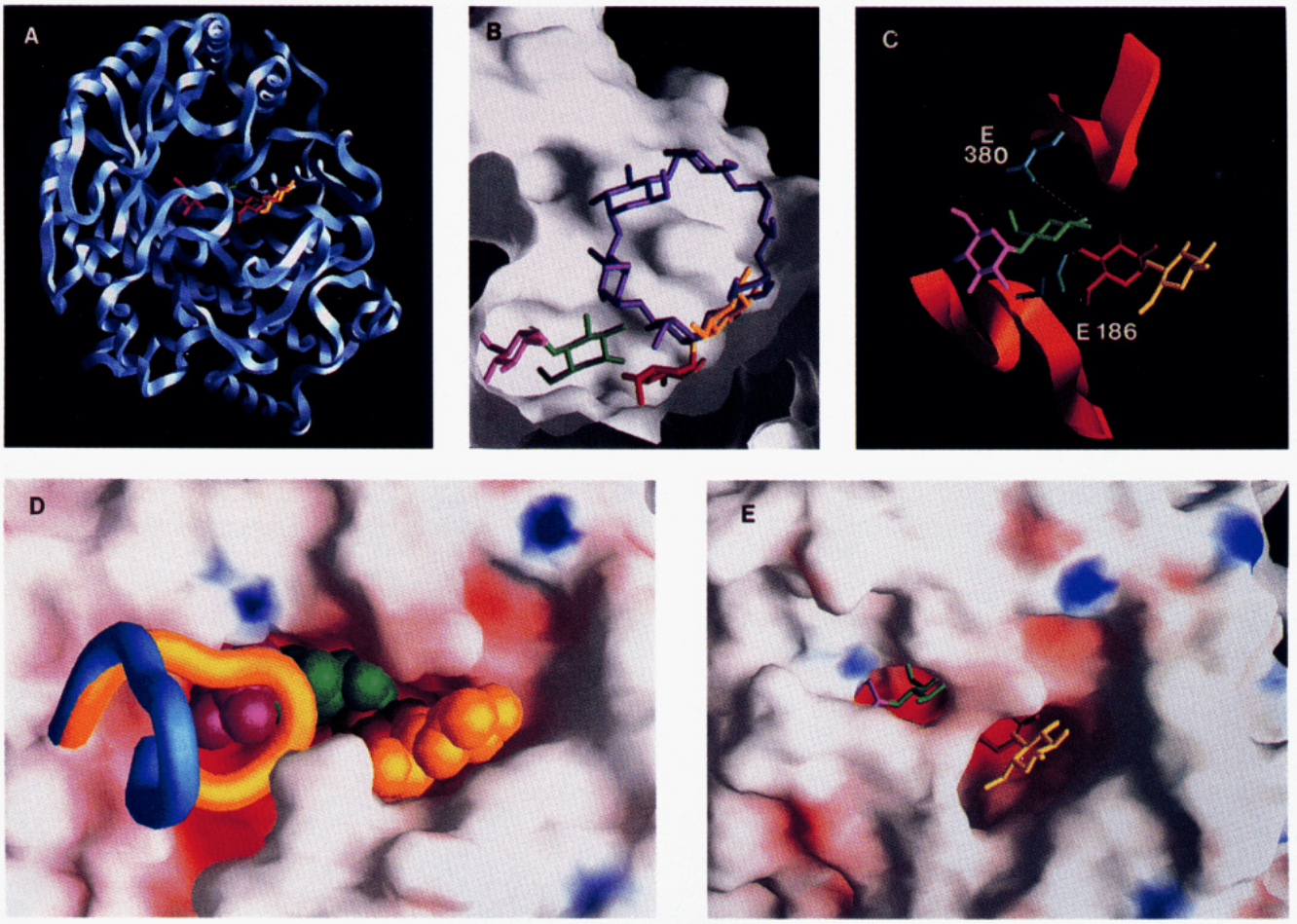


FIGURE 3: (A, top left) Ribbon diagram of soybean β-amylase soaked with β-maltose, looking toward the carboxyl end of the protein's $(\alpha/\beta)_8$ barrel core. Two molecules of β-maltose (also, in part, one of maltotetraose) are bound at the active site, partly hidden by a loop that is closed down on the ligands. The bound D-glucose residues, as they progress respectively from the most deeply seated residue (partly under a peptide shelf) to that nearest the protein surface, are designated Glc 1 (violet), Glc 2 (green), Glc 3 (red), and Glc 4 (yellow) throughout Figure 3. (B, top middle) van der Waals surface of a longitudinal section through the active site pocket, showing the dispositions of the four bound D-glucose units (e.g., of two β-maltose molecules) in the SBA/β-maltose-H complex, relative to the binding place of α-cyclodextrin complexed with a preparation of SBA having alkylated SH groups. The view is toward the small face of the bound α-cyclodextrin with the base of the active site pocket to the left. The methyl groups of Leu 383 protrude into the toroid center. (C, top right) Spatial relationship of the catalytic groups to bound ligands illustrated with the SBA/maltose-H complex: segment of loop 4 with the side chain of Glu 186 whose OE2 carboxyl oxygen (blue) is 2.6 Å from O-4 of Glc 3, and segment of β-strand 7 with the side chain of Glc 380 (blue) whose OE2 carboxyl oxygen is 2.8 Å from the *eq* O-1 of Glc 2. (D, bottom left) View into the active site pocket of the SBA/maltose-H complex showing the van der Waals protein surface (negative charges, red; positive, blue), the ligands as space-filling molecules, and "hinged" loop 3 residues 96–103 (without side chains) as tubes. Also shown is the conformation of the hinged loop in unliganded SBA (blue) and in the SBA/β-maltose-H complex (yellow). (E, bottom right) View into the active site pocket to show that the van der Waals surface extends over the reaction center when, as in the present SBA/maltose-H complex, the mobile loop 3 segment is in the closed conformation, allowing the methyl groups of one of its residues (Val 99) to interact with those of Leu 383.

Figure 3C for the SBA/maltose-H complex, the carboxyl group of Glu 186 is located below the O-5, C-1, C-2, C-3 plane of Glc 2, 2.60 Å from the O-4 atom of Glc 3; while the carboxyl group of Glu 380 is positioned above the plane of the Glc 2 ring, 2.78 Å from the equatorial O-1 atom of Glc 2. Essentially the same spatial relationships are found between these carboxyl groups and particular atoms of the bound saccharides in the SBA/maltose-L and SBA/maltal complexes (Table 2). Both glutamic acid residues are conserved in all reported plant and microbial β-amylase sequences (Mikami et al., 1993), and most important, the positional coordinates of both glutamic acid carboxyl groups are essentially unchanged in all of the present crystal structures. Spatial coordinates of the CD, OE1, and OE2 atoms of Glu 186 in unliganded SBA differed by only 0.01 or 0.02 Å (i.e., probably below the limit of accuracy of the structure model) from the coordinates of the same atoms of Glu 186 in the SBA/maltose-H, SBA/maltose-L, and SBA/maltal complexes. Likewise, the coordinates of the CD, OE1, and OE2 atoms of Glu 380 in unliganded SBA differed by only 0.01 or 0.02 Å from those of the atoms in Glu 380 in each of the SBA/ligand complexes. In contrast to the above evidence, associating the carboxyl groups of Glu 186 and Glu 380 with catalysis by β-amylase, no imidazole group is found in the immediate vicinity of the reaction center. Two imidazole groups border the active site, but that of His 93 which forms H-bonds with O-3 and O-4 of Glc 1 is 9.9 Å from O-4 of Glc 3; while that of His 300, which is hydrogen bonded to O-3 of Glc 4, is 9.0 Å from the reaction center.

*Protein/Ligand Interactions in the SBA/Saccharide Complexes.* Table 2 lists the hydrogen-bonding interactions and van der Waals contacts between protein residues and ligands in the SBA/maltose-H, SBA/maltose-L, and SBA/maltal complexes. The individual interactions of each type are strikingly similar in the three complexes. Glc 1 makes a total of seven H-bonds and seven C–C contacts (together involving Leu 20, Asp 53, Ile 89, His 93, Asp 101, Ala 184, and Arg 420). Glc 2 shows six to eight H-bonds and five C–C contacts (with Glu 186, Lys 295, Thr 342, Glu 380, Asn 381, Ala 382, and Leu 419). Glc 3 has the largest number of H-bonds,

Table 2: Ligand/Protein Interactions in Three SBA/Saccharide Complexes

| H-bond interactions (Å) | | | | | | | | C–C contacts (Å) | | | | | | | |
|---|---|---|---|---|---|---|---|---|---|---|---|---|---|---|---|
| ligand residue | | protein residue | | | SBA/ maltose-H | SBA/ maltose-L | SBA/ maltal | ligand residue[a] | | protein residue | | | SBA/ maltose-H | SBA/ maltose-L | SBA/ maltal |
| Glc 1 | O–2 | OD2 | Asp | 101 | 2.7 | 2.7 | 2.7 | Glc 1 | C-3 | Cα | Ala | 184 | 3.8 | 3.9 | 3.9 |
| | O-3 | NE2 | His | 93 | 2.9 | 2.9 | 3.0 | | C-3 | Cβ | Ala | 184 | 4.1 | 4.1 | 4.2 |
| | O-4 | OD1 | Asp | 53 | 2.6 | 2.5 | 2.5 | | C-3 | C | Ala | 184 | 4.2 | 4.2 | 4.1 |
| | O-4 | NE2 | His | 93 | 3.1 | 2.9 | 2.9 | | C-4 | CD2 | Leu | 20 | 4.4 | 4.5 | 4.6 |
| | O-5 | NE2 | Arg | 420 | 2.9 | 3.0 | 3.1 | | C-4 | CG | Asp | 53 | 4.0 | 4.0 | 4.0 |
| | O-6 | NH1 | Arg | 420 | 3.1 | 3.1 | 3.0 | | C-6 | CD1 | Ile | 89 | 3.9 | 4.0 | 4.0 |
| | O-6 | OD2 | Asp | 53 | 2.7 | 2.6 | 2.6 | | C-6 | CG | Asp | 53 | 4.1 | 4.0 | 4.1 |
| Glc 2 | O-1*eq* | OE2 | Glu | 380 | 2.8 | 2.8 | 2.9 | Glc 2 | C-1 | Cβ | Thr | 342 | 3.6 | 3.5 | 3.9 |
| | O-1*eq* | O | Asn | 381 | 2.8 | 2.9 | 2.7 | | C-2 | Cα | Ala | 382 | 4.1 | 4.2 | 4.2 |
| | O-1*eq* | O | Thr | 342 | (3.3)[b] | (3.4) | 2.9 | | C-2 | CD1 | Leu | 419 | 4.0 | 4.0 | 3.9 |
| | O-2 | O | Ala | 382 | 2.8 | 2.8 | *c* | | C-5 | CD | Glu | 186 | 4.2 | 4.2 | 4.3 |
| | O-5 | OE2 | Glu | 380 | 3.2 | (3.4) | 3.0 | | C-6 | CD | Lys | 295 | 4.0 | 4.0 | 4.1 |
| | O-5 | OG1 | Thr | 342 | (3.6) | 3.2 | (3.7) | | | | | | | | |
| | O-5 | OE2 | Glu | 186 | (3.5) | 3.2 | (3.6) | Glc 3 | C-1 | CE1 | Tyr | 192 | 4.1 | 4.0 | 4.0 |
| | O-6 | OE2 | Glu | 380 | 2.8 | 2.7 | 2.8 | | C-1 | CH2 | Trp | 301 | 3.9 | 3.9 | 3.9 |
| | O-6 | NZ | Lys | 295 | 2.8 | 3.0 | 2.9 | | C-1 | CZ3 | Trp | 301 | 4.1 | 4.1 | 4.0 |
| | | | | | | | | | C-2 | C | Gly | 298 | 4.2 | 4.2 | 4.2 |
| Glc 3 | O-2 | O | Gly | 298 | 2.8 | 3.0 | 2.7 | | C-3 | Cβ | Ala | 382 | 4.1 | 4.0 | 4.1 |
| | O-3 | N | Gly | 298 | 2.9 | 2.8 | 3.0 | | C-4 | CD | Glu | 186 | 3.8 | 3.8 | 3.9 |
| | O-3 | OG1 | Thr | 342 | 2.8 | 2.8 | 2.8 | | C-6 | OE1 | Tyr | 192 | 4.2 | 4.1 | 4.1 |
| | O-4 | OG1 | Thr | 342 | (3.3) | 3.2 | 3.2 | | C-6 | CD | Glu | 186 | 4.1 | 4.2 | 4.2 |
| | O-4 | OE2 | Glu | 186 | 2.6[d] | 2.5[d] | 2.6 | | | | | | | | |
| | O-5 | O | Tyr | 192 | 3.1 | 3.2 | 3.0 | Glc 4 | C-1 | CD1 | Leu | 383 | 4.4 | 4.2 | 4.6 |
| | O-6 | OE1 | Glu | 186 | 2.6 | 2.5 | 2.6 | | C-2 | CE2 | Met | 346 | 4.1 | 4.0 | 4.4 |
| | O-6 | O | Tyr | 192 | 2.9 | 2.8 | 2.7 | | C-2 | CD1 | Phe | 200 | 4.0 | 4.1 | 4.4 |
| | O-6 | NE | Arg | 188 | (3.3) | 3.2 | (3.4) | | C-2 | CE1 | Phe | 200 | 4.1 | 4.2 | 4.6 |
| | O-6 | NH2 | Arg | 188 | 2.8 | 2.8 | 2.7 | | C-3 | CE | Met | 346 | 3.6 | 3.5 | 4.0 |
| | | | | | | | | | C-3 | CZ3 | Trp | 301 | 4.1 | 4.1 | 4.5 |
| Glc 4 | O-3 | N | His | 300 | 2.7 | 2.8 | 2.8 | | C-3 | CD1 | Leu | 383 | 4.7 | 4.8 | 4.3 |
| | | | | | | | | | C-4 | CZ3 | Trp | 301 | 3.8 | 4.1 | 4.0 |
| | | | | | | | | | C-4 | CH2 | Trp | 301 | 3.9 | 4.3 | 4.2 |
| | | | | | | | | | C-5 | CG1 | Val | 99 | 4.4 | 4.4 | 4.3 |
| | | | | | | | | | C-6 | CH2 | Trp | 198 | 4.1 | 4.2 | 4.2 |
| | | | | | | | | | C-6 | CZ3 | Trp | 198 | 4.1 | 4.2 | 4.4 |
| | | | | | | | | | C-6 | CE1 | Tyr | 192 | 3.9 | 4.1 | 3.9 |
| | | | | | | | | | C-6 | CD1 | Tyr | 192 | 4.1 | 4.3 | 4.3 |
| | | | | | | | | | C-6 | CH2 | Trp | 301 | 4.1 | 4.2 | 4.6 |
| | | | | | | | | | C-6 | CG1 | Val | 99 | 4.2 | 4.2 | 4.2 |

[a] Sugars Glc 1–4 are numbered in the order of their disposition when bound to protein, with Glc 1 the most deeply bound sugar residue. [b] Parenthetical values, though too large to be considered H-bonds, are included for comparison with those of the other complexes. [c] Glc 2 is 2-deoxy-D-glucose in this complex. [d] The O-4 atom of Glc 3 represents that of both the 4-OH group of the second bound β-maltose molecule and the bridge oxygen atom of the 1,4-glycosidic linkage of the bound maltotetraose molecule.

Chart 1

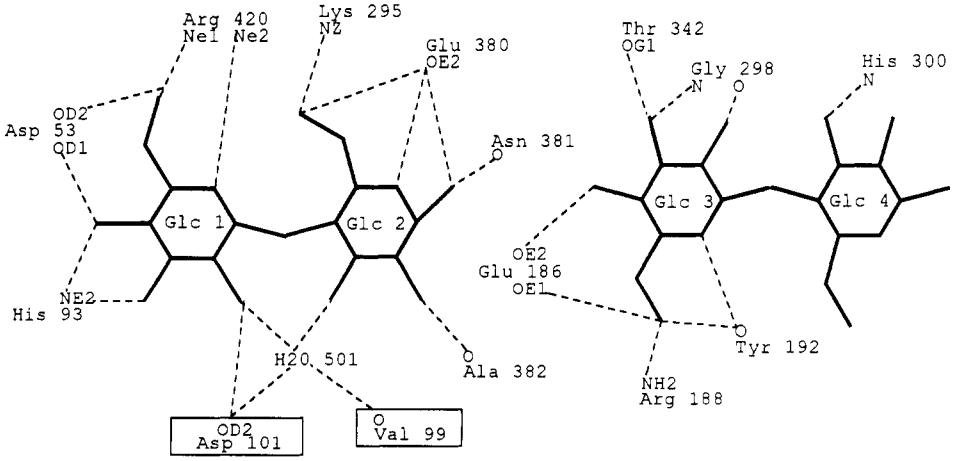


eight to ten, in addition to eight C–C contacts (with Glu 186, Arg 188, Tyr 192, Gly 298, Thr 342, Trp 301, and Ala 382). Glc 4, in contrast to all of the foregoing, shows only a single H-bond (with His 300) but a large number (16) of van der Waals contacts with Val 99, Tyr 192, Trp 198, Phe 200, Met 346, and Leu 383.

A schematic picture (Chart 1) illustrates the H-bonding interactions between protein residues and carbohydrate ligands in the SBA/β-maltose-H complex.

*Ordered Protein/Water Interactions.* We were able to localize 321 ordered solvent molecules in the unliganded SBA. Sixteen water molecules are present in the binding cavity, forming hydrogen bonds with polar side chains. Ten of these 16 waters are displaced by the substrates in all the liganded

SBA forms, eight by exocyclic oxygens of the carbohydrate ligands, one by O-5 of Glc 2, and one by C-2 of Glc 3. We found nine closed cavities in the protein interior, using the program GRASP (kindly provided by Drs. A. Nichols and B. Honig, Columbia University), all located near the edge of the $(\alpha/\beta)$ barrel. In seven of these we found electron density peaks greater than $3\sigma$, in the $[F_o] - [F_c]$ maps, and these were assigned to a total of 11 ordered water molecules; in addition, the seven cavities are surrounded by polar side chains. The two other cavities having no electron density within them are encircled by hydrophobic residues.

When the electron density present in the active site of the SBA/maltose-H and SBA/maltose-L complexes is fitted with maltotetraose (which is formed from β-maltose by condensation and is a substrate for hydrolysis by the enzyme), the subsequently calculated $[F_o] - [F_c]$ $\phi_c$ map shows a strong peak approximately in the position of the equatorial O-1 atom of Glc 2. This electron peak can be due to an ordered water molecule, $H_2O$ 866, in the maltotetraose form and/or to the O-1 hydroxyl in the β-maltose form. $H_2O$ 866 is found in unliganded SBA 2.66 Å from the OE2 of Glu 380 and 2.70 Å from the O of Asn 381 but is absent in the complexes with bound hydrolytic products, β-maltose or β-2-deoxymaltose.

*Local Conformational Change in Competent SBA Treated with Small Substrates.* A difference in the conformation of a segment of loop 3 (residues 96–103) distinguishes unliganded SBA from SBA/maltose-H, SBA/maltose-L, and SBA/maltal, which have saccharides bound at the active site, as demonstrated in Figure 3D. This views the van der Waals surface of the active site region of the SBA/maltose-H complex but with the Cα chain of the loop 3 segment displayed as a tube. That of unliganded SBA (blue) is found primarily in an open position, orthogonal to the protein surface, whereas that of the SBA/β-maltose complex (yellow) found closed over part of the bound ligand. The open conformation also differs in being considerably disordered. Mean *B*-factor values for residues 96–103 were 54 Å$^2$ for loop 3 in the open position compared to 25 Å$^2$ for all residues of unliganded SBA and 23 Å$^2$ for loop 3 in the closed position compared to 21 Å$^2$ for all residues of the same SBA/maltose-H complex.

The loop 3 segment appears to behave as a hinged lid, with residues Gly 96 and Asp 102 acting as hinges. It is evident (Figure 3D) that the approximate "planes" formed by the loop in the open and closed positions are roughly perpendicular to each other. In other words, the structure of the loop only changes its position based on rotations around the hinge. The measured Cα atom distance for individual loop residues between the major conformations in SBA and in SBA/$G_2$H differs with each residue; for Val 99 the distance is greater than 10 Å, i.e., corresponding to a traversed arc longer than 15 Å. Figure 4 illustrates the positional differences of the Cα atoms of individual loop 3 residues in SBA relative to those in the several SBA/ligand complexes. The gradually increasing displacement of amino acids from 96 to 99 and from 103 to 99 supports the view of a concerted, hinged-lid behavior of the loop 3 segment in the catalytically active protein. The lack of much difference in the loop conformation in SBA and in blocked SBA complexed with α-cyclodextrin (Mikami et al., 1993) is shown for comparison.

*Loop 3 as an Essential Part of the Active Site Structure.* Particular attention is called to the interactions of two residues of loop 3 (shown boxed in chart 1) with bound β-maltose, since these establish that loop 3 in the closed conformation forms part of the active site. These interactions include the 2.7-Å H-bond between OD2 of Asp 101 and O-2 of Glc 1 and, more indirectly, the 2.8-Å H-bond between the O of Val 99

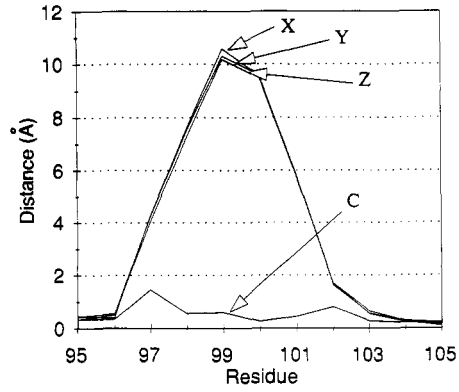


FIGURE 4: Differences in the positions of Cα atoms of individual amino acid residues of loop 3 in the open conformation in unliganded SBA and loop 3 in the closed conformation in SBA/maltal (X), SBA/maltose-H (Y), and SBA/maltose-L (Z). Differences between the residues in unliganded SBA and the inactivated SBA/α-cyclodextrin complex (C) are shown for comparison.

and $H_2O$ 501, which is in turn H-bonded to O-2 of Glc 1 and to O-3 of Glc 2. van der Waals contacts between CG1 of Val 99 and C-5 and C-6 of Glc 4 are not shown in Chart 1.

In addition, loop 3 in the closed conformation forms part of a structural cover over parts of the ligands and reaction center that otherwise would be exposed to solvent. Figure 3E shows the van der Waals surface of the active site region of SBA/maltose-H, with loop 3 in the closed conformation and glucose ligands positioned as in all three SBA/saccharide complexes. The C–C interaction between the methyl groups of Val 99 and those of Leu 383 emphasizes the hydrophobic nature of the layer that, with loop 3 closed, shields the reaction center from solvent. Access to solvent, measured in the SBA/maltose-H complex using GRASP, using a spherical probe of 1.4-Å radius (Connolly, 1983), gave values for Glc 1 to Glc 4 of 0, 5.9, 10.9, and 70.3 Å$^2$, respectively; for C-1 or *eq* O-1 of Glc 2, 0 Å$^2$; for C-4 or O-4 of Glc 3, 0 Å$^2$; and for the side chain of either Glu 186 or Glu 380, 0 Å$^2$. In contrast, access to solvent of the side chain of Glu 186 and Glu 380 in unliganded SBA measured 27.6 and 36.7 Å$^2$, respectively.

## DISCUSSION

Analyses of the 1.9–2.2-Å-resolution structures of active soybean β-amylase, using crystals soaked in half-saturated ammonium sulfate solution alone or containing freshly dissolved β-maltose or maltal, provide the first detailed description of the enzyme's active site composition and geometry. The findings are of particular interest for the insights they furnish into the relationships of structural features to specific aspects of catalysis recorded for this classic enzyme.

The sugar residues bound in the SBA complexes prepared with β-maltose or maltal occupy four successive positions in the active site. This number of subsites was originally proposed for β-amylase by Thoma and Koshland (1960a) on the basis that the enzyme hydrolyzes maltotetraose nearly as fast as higher maltosaccharides. We find no evidence for more than four subsites but envision that with substrate chains longer than the tetrasaccharide several additional glucose moieties will interact with the protein, possibly through hydrophobic C–C contacts with the methyl groups of Leu 383 as found with glucosyl residues of α-cyclodextrin that interact near the protein surface (Mikami et al., 1993). Suganuma et al. (1980), Isoda and Nitta (1986), and Kunikata et al. (1992) report the presence of more than four subsites in SBA, with only the first and fourth glucose units from the nonreducing end of maltosaccharides having a high binding affinity. We observe that Glc 1 and Glc 4 in both SBA/β-maltose complexes do

show more highly ordered electron density patterns than Glc 2 and Glc 3. However, contrary to the conclusion of Kunikata et al. (1992) that only one maltose molecule binds in the active site of SBA (and only in a nonproductive manner), two β-maltose molecules plus their condensation product are clearly present even in SBA treated with a modest (8 mM) concentration of β-maltose.

Present findings identify the carboxyl groups of two glutamic acid residues, Glu 186 and Glu 380, as the probable catalytic groups in SBA. Both residues are conserved in all reported plant and microbial β-amylase sequences (Mikami et al., 1993). In early pH/$K_m$ studies, Thoma and Koshland (1960b) and Thoma et al. (1965) found two ionizing groups whose p$K_a$ constants were thought to implicate a carboxyl and a protonated imidazole group in catalysis by sweet potato β-amylase. Zherebetsov (1968) reported heats of ionization pointing to the same two catalytic groups in barley β-amylase. Indeed, a catalytic role for imidazole has been generally accepted. However, Hoschke et al. (1980) found only a drop in substrate binding affinity and no significant change in activity following the ethoxycarbonylation of the histidine residues of β-amylase. They concluded that a protonated carboxyl group (rather than a protonated imidazole) is the catalytic group responsible for the higher p$K_a$ value observed by Thoma and Koshland (1960a). In SBA two histidine residues border the active site (His 93 interacts with Glc 1 and His 300 with Glc 4), but their imidazole groups are too remote from the reaction center to be significantly involved in the catalytic chemistry (Chart 1); at best, they might perhaps provide some secondary assiatance in transition-state stabilization.

Of the two carboxyl groups now shown to occur in appropriate spatial relationship to reactants at the catalytic center, that of Glu 186 was identified as a likely catalytic group by fragmentation studies of SBA labeled with the inhibitor 2,3-epoxypropyl α-D-[$^{14}$C]glucopyranoside (Nitta et al., 1989). The likelihood was enhanced by our finding (Mikami et al., 1993) that this carboxyl group is located in the active pocket of the protein, below where α-cyclodextrin binds. Isoda and Nitta (1986, 1988) had reported that a carboxylate group of p$K_a$ 3.5 and either a protonated imidazole group of histidine or and ε-amino of lysine (p$K_a$ 8.2) participate in the inhibition. Nitta et al. (1989) deduced that the labeled Glu 186 group is the same carboxylate that would function with p$K_a$ 3.5 in maltosaccharide hydrolysis. These authors did not consider that the carboxyl of Glu 186, rather than the imidazole of histidine or the ε-amino group of lysine, might function as a general acid and proton donor, with p$K_a$ 8.2, in hydrolyzing α-1,4-glucosidic linkages. The carboxyl group of Glu 186 is, in fact (Figure 3C), located below the *si*-face of Glc 2, 2.6 Å from the O-4 atom of Glc 3 (equivalent to the oxygen atom of the penultimate α-glycosidic linkage in bound maltotetraose). The carboxyl group of Glu 380 is located above the *re*-face of Glc 2, 2.8 Å from the *eq* O-1 hydroxyl of this reducing unit of the more deeply bound β-maltose or β-2-deoxymaltose.

Glu 380 presumably acts as a general acid in the observed condensation of β-maltose to form maltotetraose and $H_2O$ 866 and in the hydration of maltal to form β-2-deoxymaltose. Although bound unreacted maltal substrate was not observed, maltal could be fitted into "subsites" 1 and 2 with its double bond positioned close enough to the carboxyl group of Glu 380 to elevate its p$K_a$ and to be protonated "from above" as demonstrated in $^1$H NMR experiments (Hehre et al., 1986; Kitahata et al., 1991). In any case two opposing carboxyl groups, as first observed with hen's egg lysozyme, appear to comprise the catalytic elements of β-amylase and glycosylases generally, in contrast to the catalytic nucleophile–histidine–acid triad found in the α/β hydrolase-fold family of enzymes (Ollis et al., 1992).

Stability of the coordinates of Glu 186 and Glu 380 in SBA and the three SBA complexes shows that the spatial relationship of Glu 186 and Glu 380 to each other is not affected by ligand binding, contrary to the view of Thoma and Koshland (1960a) that substrates for β-amylase induce the catalytic groups to move into proper alignment. Their assumption that α-cyclodextrin acts as an inhibitor by competing with substrates for binding sites closely associated with the catalytic groups also is not supported (Figure 3B).

Numerous protein/ligand interactions are involved in binding the present small substrates and/or their reaction products and, thus, in defining the active site of SBA (Table 2). Hydrogen binding O–O or O–N interactions within 3.2 Å predominant with Glc 1, 2, and 3, whereas van der Waals C–C contacts within 4.5 Å predominate with Glc 4. Of particular significance is that two residues of loop 3 in the closed conformation interact with ligands and thus make the closed loop part of the active site. In each of the SBA/saccharide complexes examined, the carboxyl group of Asp 101 forms a H-bond with O-2 of Glc 1, while the CG1 of Val 99 forms van der Waals contacts with C-5 and C-6 of Glc 4; the carbonyl group of Val 99 also interacts with ligands indirectly via a hydrogen bond to $H_2O$ 501 which, in turn, forms a H-bond with O-2 of Glc 1 and O-3 of Glc 2. An important additional finding (manuscript in preparation) is the apparent downward displacement of C-2, C-1, and O-1 of bound Glc 2 with loop 3 in the closed configuration, relative to the positions of these atoms of Glc 2 in complexes involving SBA inactivated by alkylation of its –SH groups, where no interactions are observed between the sugar ligands and residues Val 99 and Asp 101 of loop 3. We envision the possibility that loop 3 in the closed conformation may displace Glc 2 toward a more reactive conformation.

The mobile hinged loop 3 segment bordering the active site in SBA closely resembles the hinged loop in triosephosphate iosmerase (Alber et al., 1983; Joseph et al., 1990). The mobile loop in β-amylase is clearly a solution structure with no crystal lattice contact. The distance between the main-chain atoms of residues 96–103 and the closest neighboring protein molecule is of the order of 10 Å (loop open) or 15 Å (loop closed). We assume, as envisioned for triosephosphate isomerase (Alber et al., 1983), that the mobile loop in β-amylase exists as an equilibrium among a number of different conformations. In crystalline unliganded SBA, the predominant conformation extends into solvent, but at least one additional conformation of the loop exists near or at the active site. The loop in this infrequent closed position becomes favored as substrate is introduced, causing the conformational equilibrium to shift from one favoring open positions to one favoring the closed conformation. Thus, no special signal is needed to close the lid on the active site or to open it in order for product to be released.

Present structural findings are consistent with catalysis of the hydrolysis of the penultimate α-1,4-glycosidic linkage of maltosaccharides, in which the carboxyl group of Glu 186 acts as a general acid and the carboxylate of Glu 380 serves as a general base, and also with the reverse condensation, involving β-maltose as glycosyl donor plus a second maltose residue to form maltotetraose and a molecular of water, in which the roles of Glu 186 and Glu 380 are reversed in accord with the principle of microscopic reversibility. With respect to maltal hydration, the results are in keeping with the reported

protonation of the double bond from "above" (Hehre et al., 1986; Kitahata et al., 1991) in that the carboxyl group of Glu 380 appears able to have its $pK_a$ elevated by proximity to the double bond and to act as a general acid catalyst. Especially significant is that the findings confirm that β-amylase hydrates maltal to form β-2-deoxymaltose, providing strong evidence (Kitahata et al., 1991) that product configuration is topologically controlled and is not ordained by substrate configuration and that in starch hydrolysis the same protein structures likewise control the entry of water specifically from the β-side of the reaction center. Present findings provide the first insights into the likely manner whereby β-amylase achieves topological control of product configuration in hydrolytic reactions. First, loop 3 closure not only tightens substrate binding but also shields the reaction center from solvent through hydrophobic contacts between the methyl groups of Val 99 and Leu 383. The reactant water molecule must therefore exist below this van der Waals surface prior to loop 3 closure. Ordered $H_2O$ 866, present in unliganded SBA 2.7 Å from both the OE2 carboxyl group of Glu 380 and the main-chain O atom of Asn 381, could well be the reactant in the hydrolytic reactions catalyzed by β-amylase. $H_2O$ 866 disappears on the hydration of maltal, its place taken by the *eq* O-1 atom of the β-2-deoxymaltose hydration product. $H_2O$ 866 is also absent in the SBA/maltose-H and -L complexes where it is displaced to solvent by the *eq* O-1 atom of the bound β-maltose substrate. Finally, as a product of the condensation synthesis of maltotetraose in these complexes, $H_2O$ 866 appears in the same place, 2.7 Å from the OE2 carboxyl of Glu 380 and the main-chain oxygen of Asn 381. No comparable ordered water is present near Glu 186.

One may envision an α-1,4-linked outer chain of amylopectin bound at the active site of β-amylase with the four terminal glucose residues occupying subsites 1–4; the binding of these residues includes interactions with residues of loop 3 in the closed conformation. Following the catalyzed chemical event of hydrolytic cleavage of the penultimate glycosidic linkage, β-maltose and a shortened outer chain of amylopectin are formed. However, the maltose product cannot be released to solvent with the loop 3 segment in the closed conformation, and its departure provides one point of evidence that loop 3 mobility is essential to productive catalysis by β-amylase. With loop 3 returned to the open position, possibly assisting maltose ejection through the H-bond between Asp 101 and O-2 of Glc 1, the binding of the shortened remainder of the amylopectin chain is weakened by loss of more than a dozen H-bond interactions (Chart 1) to the extent that the chain may begin to disengage from the protein. It would then appear possible that Brownian movement-driven translation of the residual chain toward the base of the active site pocket may occur, guided by multiple hydrophobic contacts between Tyr 301, Phe 200, and Leu 383 and residues Glc 3, Glc 4, and beyond. The methyl groups of Leu 383, especially, might tend to hold the residual outer chain in a loose left-hand helix conformation to assist feeding the new nonreducing end maltose unit into position for a repeated attack. Model building studies indicate that this maltose residue cannot be fitted into subsites 1 and 2 if the next D-glucose unit of the chain is a branch point molecule carrying an α-D-glucosyl or larger substituent at O-6.

## REFERENCES


Alber, T., Banner, D. W., Bloomer, A. C., Petsko, G. A., Phillips, D., Rivers, P. S., & Wilson, I. A. (1981) *Philos. Trans. R. Soc. London, B 293*, 159–171.

Alber, T., Gilbert, N. A., Ponzi, D. R., & Petsko, G. A. (1983) *Ciba Found. Symp. 93*, 4–18 (4–24 with discussion).

Aleshin, A., Golubev, A., Firsov, L. M., & Honzaiko, R. B. (1992) *J. Biol. Chem. 267*, 19291–19298.

Bailey, J. M., & French, D. (1957) *J. Biol. Chem. 226*, 1–14.

Brünger, A. T. (1992) *XPLOR Version 3.1 Manual: A System for Crystallography and NMR*, Yale University, New Haven, CT.

Brünger, A. T., Kuriyan, J., & Karplus, M. (1987) *Science 35*, 458–460.

Buisson, G., Duee, E., Haser, R., & Payen, F. (1987) *EMBO J. 6*, 3909–3916.

Connolly, M. L. (1983) *J. Appl. Crystallogr. 16*, 548–558.

Genghof, D. S., Brewer, C. F., & Hehre, E. J. (1978) *Carbohydr. Res. 61*, 291–299.

Greenwood, C. T., & Milne, E. A. (1968) *Adv. Carbohydr. Chem. 23*, 281–386.

Hehre, E. J., Okada, G., & Genghof, D. S. (1969) *Arch. Biochem. Biophys. 135*, 75–89.

Hehre, E. J., Genghof, D. S., Steinlicht, H. E., & Brewer, C. F. (1979) *J. Biol. Chem. 254*, 5942–5950.

Hehre, E. J., Kitahata, S., & Brewer, C. F. (1986) *J. Biol. Chem. 261*, 2147–2153.

Hoschke, A., Laszlo, E., & Hollo, J. (1980) *Carbohydr. Res. 81*, 145–146.

Isoda, Y., & Nitta, Y. (1986) *J. Biochem. (Tokyo) 99*, 1631–1637.

Isoda, Y., & Nitta, Y. (1988) *Agric. Biol. Chem. 52*, 271–272.

Jones, T. A. (1985) *Methods Enzymol. 115*, 157–171.

Joseph, D., Petsko, G. A., & Karplus, M. (1990) *Science 249*, 1425–1428.

Kato, M., Hiromi, K., & Morita, Y. (1974) *J. Biochem. (Tokyo) 75*, 563–576.

Kitahata, S., Chiba, S., Brewer, C. F., & Hehre, E. J. (1991) *Biochemistry 30*, 6769–6775.

Kunikata, T., Yamano, H., Nagamura, T., & Nitta, Y. (1992) *J. Biochem. (Tokyo) 112*, 421–425.

Marshall, J. J., & Whelan, W. J. (1973) *Anal. Biochem. 52*, 642–646.

Matsuura, Y., Kusunoki, H., Harada, W., & Kakudo, M. (1984) *J. Biochem. (Tokyo) 95*, 697–702.

Meyer, K. H., Wertheim, M., & Bernfeld, P. (1941) *Helv. Chim. Acta 24*, 212–216.

Mikami, B., Shibata, T., Hirose, M., Aibara S., Sato, M., Katsube, Y., & Morita, Y. (1992) *J. Biochem. (Tokyo) 112*, 541–546.

Mikami, B., Hehre, E. J., Sato, M., Katsube, Y., Hirose, M., Morita, Y., & Sacchettini, J. C. (1993) *Biochemistry 32*, 6836–6845.

Nitta, Y., Isoda, Y., Toda, H., & Sakiyama, F. (1989) *J. Biochem. (Toyko) 105*, 573–576.

Ollis, D. L., Cheah, E., Cygler, M., Dijkstra, B., Frolow, F., Franken, S. M., Harel, M., Remington, S. J., Silman, I., Schrag, J., Sussman, J. L., Verschuren, K. H. G., & Goldman, A. (1992) *Protein Eng. 5*, 197–211.

Smith, J. L., Corfield, P. W. R., Hendrickson, W. A., & Low, B. W. (1988) *Acta Crystallogr., Sect. A 44*, 357–368.

Suganuma, T., Ohnishi, M., Hiromi, K., & Morita, Y. (1980) *Agric. Biol. Chem. 44*, 1111–1117.

Sumner, R., & French, D. (1956) *J. Biol. Chem. 222*, 469–477.

Thoma, J. A., & Koshland, D. E. (1960a) *J. Am. Chem. Soc. 82*, 3329–3333.

Thoma, J. A., & Koshland, D. E. (1960b) *J. Mol. Biol. 2*, 169–170.

Thoma, J. A., Koshland, D. E., Shinke, R., & Ruscica, J. (1965) *Biochemistry 4*, 714–722.

Tronrud, D. E., Ten Eyck, L. F., & Mathews, B. W. (1988) *Acta Crystallogr., Sect. A 43*, 489–501.

Zherebetsov, N. A. (1968) *Biokhimiya 33*, 435–444.